A scaling approach for interacting quantum wires—a possible explanation for the 0.7 anomalous conductance

2010 J. Phys.: Condens. Matter 22 095301

(http://iopscience.iop.org/0953-8984/22/9/095301)

J. Phys.: Condens. Matter **22** (2010) 095301 (10pp) doi:10.1088/0953-8984/22/9/095301

A scaling approach for interacting quantum wires—a possible explanation for the 0.7 anomalous conductance

D Schmeltzer[1], **A Kuklov**[2] **and M Malard**[3]

[1] Department of Physics, City College of the CUNY, USA
[2] Physics Department at the College of Staten Island of the CUNY, USA
[3] International Center for Condensed Matter Physics, Brasilia, Brazil

Received 24 December 2009
Published 10 February 2010
Online at stacks.iop.org/JPhysCM/22/095301

Abstract

We consider a weakly interacting finite wire with short and long range interactions. The long range interactions enhance the $4k_F$ scattering and renormalize the wire to a strongly interacting limit. For large screening lengths, the renormalized charge stiffness Luttinger parameter $K_{\rm eff}$ decreases to $K_{\rm eff} < \frac{1}{2}$, giving rise to a Wigner crystal at $T = 0$ with an anomalous conductance at finite temperatures. For short screening lengths, the renormalized Luttinger parameter $K_{\rm eff}$ is restricted to $\frac{1}{2} \leqslant K_{\rm eff} \leqslant 1$. As a result, at temperatures larger than the magnetic exchange energy we find an interacting metal which, for $K_{\rm eff} \approx \frac{1}{2}$, is equivalent to the Hubbard $U \to \infty$ model, with the anomalous conductance $G \approx \frac{e^2}{h}$.

(Some figures in this article are in colour only in the electronic version)

1. Introduction

The anomalous conductance $G \approx 0.7 \times (2e^2/h)$ discovered by Pepper *et al* [1] and further investigated by [2–6] is one of the major unexplained effects in quantum wires. Several theories have been proposed: phenomenological theories [7, 8], the Kondo effect [4], spin polarization [9, 10], formation of bound states [5], unrestricted Hartree–Fock calculations for point contacts [11], Wigner crystal [12], ferromagnetic spin coupling [13], ferromagnetic zigzag structures [14], the spin incoherent Luttinger liquid [15–17], and the formation of a quasi-localized state [18]; however no consensus has been reached.

For non-interacting spin unpolarized electrons, the conductance of narrow ballistic quantum wires connected to two (large) reservoirs is quantized in units of $2e^2/h$. An early suggestion was that the electron–electron interaction should modify the conductance for a Luttinger liquid [19, 20] as $K(2e^2/h)$ where K is interaction-dependent. Using the method of bosonization for weakly interacting fermions, it has been shown that by taking first the frequency limit $\omega \to 0$ before the momentum limit $q \to 0$, the non-interacting leads modify the metallic conductance to the limit $G = \frac{2e^2}{h}$ [21–23].

GaAs/AlGaAs in the lowest populated conduction band is a weakly interacting metal characterized by the Luttinger liquid charge $K \leqslant 1$ and spin $K_s \approx 1$ parameters. The presence of the unscreened, long range Coulomb interaction (in a one-dimensional wire) alters this picture. From our renormalization group study [24] we find that the Coulomb long range interaction enhances the weak $4k_F$ scattering channel and decreases the Luttinger charge parameter to $K_{\rm eff} \ll 1$. As a function of the screening length, we can have either a strongly interacting metal (similar to the Hubbard $U = \infty$ model) or an insulating Wigner crystal. In order to capture both phases, we investigate a microscopic model of a wire of length L with a lattice constant a in the presence of a weak scattering potential. The lattice constant a is much smaller than the transverse width d of the wire, which controls the low energy excitations in the lowest band. The effective model in the lowest band is given by the renormalized lattice model. This is achieved by a real space renormalization group procedure, which replaces the discrete lattice model (lattice constant a) by the new lattice constant $d = \text{integer} \times a$, and renormalized interaction coupling constants. The effective model at the length scale d will be a function of the microscopic Fermi momentum k_F (defined by the electronic density) and the effective umklapp momentum $G^{(d)}$, obeying the relation $G^{(d)} \cdot d = G^{(a)} \cdot a$, where $G^{(a)}$ is the microscopic umklapp vector. At the length scale d, the long range interaction is separated into two parts: the large momentum transfer, included in the

effective short range Hubbard interaction, and the *forward* Coulomb interaction. The forward Coulomb interaction gives rise to $4k_F = G^{(\mathrm{Wigner})} = \frac{2\pi}{r_{e-e}}$ oscillations [25], where r_{e-e} is the inter-particle distance. At $T = 0$, a Wigner crystal ground state with a charge gap Δ is formed if the effective charge parameter obeys $K_{\mathrm{eff}} < \frac{1}{2}$. At finite temperatures, comparable to the charge gap Δ, the conductance is given by $G \approx \frac{e^2}{h}$. For short screening lengths, the interacting parameter K_{eff} is restricted to $\frac{1}{2} \leqslant K_{\mathrm{eff}} < 1$. As a result, we find that at finite temperatures which are larger than the magnetic exchange energy, the limit $K_{\mathrm{eff}} \approx \frac{1}{2}$ is equivalent to the Hubbard $U = \infty$ model. Therefore, at finite temperatures we find the conductance is given by $G \approx \frac{e^2}{h}$.

The plan of this paper is as follow: in section 2, we present the interacting fermion model. The renormalization effects for the finite wire will be investigated in section 3 using the zero mode formulation [22, 26, 27]. In section 4, we present the fermion–boson representation for the interacting wire. In section 5, we present the renormalization group (RG) analysis and show that the renormalization effects of the effective charge interaction parameter K_{eff} are controlled by the electronic density and screening length. In section 6, we use the renormalized interaction parameters to compute the effective zero mode Hamiltonian at finite temperatures for $\frac{1}{2} \leqslant K_{\mathrm{eff}} < 1$. Section 7 is dedicated to the computation of the conductance at finite temperatures for $\frac{1}{2} \leqslant K_{\mathrm{eff}} < 1$. In section 8, we consider the case $\frac{1}{2} \approx K_{\mathrm{eff}}$ and show that the model is equivalent to the incoherent Luttinger liquid, which emerges at finite temperatures for the Hubbard $U \to \infty$ model. In section 9, we consider the case $K_{\mathrm{eff}} < \frac{1}{2}$, which at zero temperature gives rise to a Wigner crystal with a charge density wave gap Δ. In section 10, we present our numerical results using the experimental parameters given by [3]. In section 11, we examine the effect of the Zeeman interaction. Section 12 is devoted to conclusions. Appendix A deals with the thermodynamics of the zero modes, and in appendix B we present the calculation of the self-energy for a wire of length $L \approx 10^{-6}$ at temperatures $T \approx 1$ K.

2. The model

We consider an interacting wire at low electronic densities that has a finite width d. The geometric parameters in the quantum wire experiments are: the gate screening length $\xi = 10^{-7}$ m, the wire length $L \approx 10^{-6}$ m, the width $d \approx \frac{L}{100}$, the two-dimensional carrier density $n_s \approx 2.5 \times 10^{11}$ cm^{-2} and the electronic lattice spacing $a \approx 10^{-10}$ m. Due to the width d, the single particle excitations are characterized by a set of electronic bands with the transverse quantization energies $\frac{\hbar^2}{2m*}\frac{(r^2)\pi^2}{d^2}$, $r = 1, 2, 3 \ldots$. The gate voltage is such that, at the temperatures considered in the experiment, only the *lowest band* is populated. In order to describe the low energy physics, we project the microscopic Hamiltonian H^a (the microscopic model defined at the lattice scale a) into the lowest band. As a result, the effective one-dimensional Hamiltonian H with the energy cut-off characterized by the transversal energy separation $\frac{\hbar^2}{2m*}\frac{\pi^2}{d^2}$ and the momentum cut-off $\Lambda = \frac{2\pi}{d}$ preserve the original form of the microscopic Hamiltonian H^a:

$$\begin{aligned} H = & -t_d \sum_n \sum_{\sigma=\uparrow,\downarrow} (\psi^+_\sigma((n+1)d)\psi_\sigma(nd) + \mathrm{h.c.}) \\ & - \epsilon_F \sum_n \sum_{\sigma=\uparrow,\downarrow} \psi^+_\sigma(nd)\psi_\sigma(nd) \\ & + \hat{U} \sum_n \psi^+_\downarrow(nd)\psi_\downarrow(nd)\psi^+_\uparrow(nd)\psi_\uparrow(nd) \\ & + \sum_n \sum_{n' \neq n} \sum_{\sigma=\uparrow,\downarrow} \sum_{\sigma'=\uparrow,\downarrow} \psi^+_\sigma(nd)\psi_\sigma(nd) V^{(c)} \\ & \times (|nd - n'd|)\psi^+_{\sigma'}(n'd)\psi_{\sigma'}(n'd) \end{aligned} \tag{1}$$

where $t_d \approx \frac{\hbar^2}{2m*d^2}$ is the effective hopping at the length scale d, and $\hat{U}$ is the projected repulsive Hubbard interaction, which also contains the effect of the Coulomb interaction obtained by projecting out states with a lattice spacing in the interval a–d. $V^{(c)}(|nd - n'd|) = \frac{e^2}{\sqrt{(n-n')^2d^2+d^2}} - \frac{e^2}{\sqrt{(n-n')^2d^2+\xi^2}}$ is the effective long range Coulomb interaction defined for distances $x > d$ and ξ is the screening length. The Hubbard model is characterized by the particle–hole charge and spin excitations: $K \leqslant 1$ (charge) and $K_s \geqslant 1$ (spin). We consider the situation where the Fermi momentum $k_F(V_G)$ satisfies the condition $4k_F(V_G) \neq G^d \equiv \frac{2\pi}{d}$, $r_{e-e} > d$, suggesting that the umklapp interaction is negligible. According to [3], the density is expressed in terms of the external gate voltage V_G: $k_F(V_G) = \frac{\pi}{2}n_e(V_G) = \frac{C_a}{e}(V_G - V^{\mathrm{th}})$, where V^{th} is the gate voltage at which the wire is pinched off and $\frac{C_a}{e}$ is the effective capacitance. The results reported in [3] show that the conductance decreases with the lowering of the gate voltage, suggesting that the umklapp interaction is significantly enhanced. The low energy properties of the model will be investigated using a combined method of bosonization and RG theory. At finite temperatures, the exact description of the electron excitations requires the inclusion of the *zero modes* operators.

3. The representation of the electron operator for a wire of length L

The electron is represented as a product of two operators, a *bosonic* one (this is the standard bosonic representation for spin-charge excitations) and a *fermionic-zero mode* operator, which carries the electron number (electrons with spin up or spin down that are added or removed from the Fermi surface). The electron operator $\psi^+_\sigma(x)$ is restricted by the momentum with a momentum cut-off $[\Lambda, -\Lambda]$ around the Fermi surface and is given in terms of the right $R_\sigma(x)$ and left $L_\sigma(x)$ components: $\psi_\sigma(x) = \mathrm{e}^{\mathrm{i}k_F x}R_\sigma(x) + \mathrm{e}^{-\mathrm{i}k_F x}L_\sigma(x)$ with the Fermi momentum $k_F = k_F(V_G)$. We replace the right (left) mover fermion by a product of a fermion operator $F_{R,\sigma}(x)$ ($F_{L,\sigma}(x)$) and the boson operator $\mathrm{e}^{\mathrm{i}\sqrt{4\pi}\Theta_{R,\sigma}(x)}$ ($\mathrm{e}^{\mathrm{i}\sqrt{4\pi}\Theta_{L,\sigma}(x)}$):

$$\begin{aligned} R_\sigma(x) &= \sqrt{\frac{\Lambda}{2\pi}}\mathrm{e}^{\mathrm{i}\alpha_{R,\sigma}}\mathrm{e}^{\mathrm{i}(2\pi/L)(\hat{N}_{R,\sigma}-1/2)x}\mathrm{e}^{\mathrm{i}\sqrt{4\pi}\Theta_{R,\sigma}(x)} \\ &\equiv F_{R,\sigma}(x)\mathrm{e}^{\mathrm{i}\sqrt{4\pi}\Theta_{R,\sigma}(x)} \end{aligned} \tag{2}$$

$$\begin{aligned} L_\sigma(x) &= \sqrt{\frac{\Lambda}{2\pi}}\mathrm{e}^{-\mathrm{i}\alpha_{L,\sigma}}\mathrm{e}^{-\mathrm{i}(2\pi/L)(\hat{N}_{L,\sigma}-1/2)x}\mathrm{e}^{-\mathrm{i}\sqrt{4\pi}\Theta_{L,\sigma}(x)} \\ &\equiv F_{L,\sigma}(x)\mathrm{e}^{-\mathrm{i}\sqrt{4\pi}\Theta_{L,\sigma}(x)} \end{aligned} \tag{3}$$

where $e^{i\sqrt{4\pi}\Theta_{R,\sigma}(x)}$ and $e^{-i\sqrt{4\pi}\Theta_{L,\sigma}(x)}$ are the standard bosonization formulae used in the literature. $F_{R,\sigma}(x)$ and $F_{L,\sigma}(x)$ are the zero mode fermion operators that can change the number of particles and are crucial for enforcing the Fermi statistics. These operators are defined with respect to the non-interacting ground state $|F\rangle$ (the Fermi sea characterized by the Fermi momentum). The electronic Hilbert space excitations above the Fermi sea are given by the states [22, 26]: $|N_{R,\sigma}; m_q\rangle \otimes |N_{L,\sigma}; m'_q\rangle$, where $m_q \geqslant 0$, $m'_q \geqslant 0$ are integers which specify the number of bosonic quanta (particle–hole excitations) with a momentum $q = \frac{2\pi}{L} n_q > 0$. $\hat{N}_{R,\sigma}$, $\hat{N}_{L,\sigma}$ represent the change of the total number of electrons in the right and left ground states. The formal proof that relates the electron operator to the zero mode operators is given by the Jacobi identity [27]. The bosonic particle–hole excitations [22, 26] are given by: $\Theta_{R,\sigma}(x) = \Theta_\sigma(x) - \Phi_\sigma(x)$, $\Theta_{L,\sigma}(x) = \Theta_\sigma(x) + \Phi_\sigma(x)$. The zero mode fermion excitations are given in terms of the zero mode coordinates $\alpha_{R,\sigma}, \alpha_{L,\sigma}$ and their canonical conjugate fermion number operators $\hat{N}_{R,\sigma}$, $\hat{N}_{L,\sigma}$ ($\sigma = \uparrow, \downarrow$). The physics of the zero modes is described in terms of the *charge* operator $\hat{Q}_c = \sum_{\sigma=\downarrow,\uparrow}[\hat{N}_{R,\sigma} + \hat{N}_{L,\sigma}]$ and the *magnetization* operator $\hat{Q}_s = [(\hat{N}_{R,\sigma=\uparrow} + \hat{N}_{L,\sigma=\uparrow}) - (\hat{N}_{R,\sigma=\downarrow} + \hat{N}_{L,\sigma=\downarrow})]$. The canonical conjugate variables to the *charge* and *magnetization* are given by the *charge coordinate* $\hat{\alpha} = \sum_{\sigma=\downarrow,\uparrow}[\alpha_{R,\sigma} + \alpha_{L,\sigma}]$ and the *magnetization coordinate* $\hat{\alpha}_s = [(\alpha_{R,\sigma=\uparrow} + \alpha_{L,\sigma=\uparrow}) - (\alpha_{R,\sigma=\downarrow} + \alpha_{L,\sigma=\downarrow})]$. The zero modes obey the commutation rules: $[\alpha_{R,\sigma}, \hat{N}_{R,\sigma'}] = i\delta_{\sigma,\sigma'}$, $[-\alpha_{L,\sigma}, \hat{N}_{L,\sigma'}] = i\delta_{\sigma,\sigma'}$ and $[\alpha_{R,\sigma}, \hat{N}_{L,\sigma'}] = [\alpha_{L,\sigma}, \hat{N}_{R,\sigma'}] = 0$.

4. The model Hamiltonian in the boson–fermion representation

The Bethe ansatz formulation [28] and equations (2) and (3) allow us to map equation (1) into a charge and spin interacting model. The mapping is a function of the Hubbard interaction strength $U \equiv \frac{\hat{U}}{t_d}$ and the electronic density n_e. The Hamiltonian is controlled by the charge parameter $K = K(U, n_e)$, spin parameter $K_s = K(U, n_e)$, umklapp interaction $g = g(U, n_e) = \hat{g}\Lambda^2$, spin backward scattering parameter $g_s = g(U, n_e) = \hat{g}_s\Lambda^2$, Fermi velocity v_F, charge density wave velocity $v = v(U, n_e)$ and the spin density wave velocity $v_s = v_s(U, n_e)$. The Hamiltonian in equation (1) is replaced by: $H = H_c^{n\neq 0} + H_s^{n\neq 0} + H^{(n=0)}$. The first two Hamiltonians $H_c^{n\neq 0} + H_s^{n\neq 0}$ represent the particle–hole excitations and $H^{(n=0)}$ represents the zero modes. The charge excitations $H_c^{n\neq 0}(\Theta, \Phi; \hat{\alpha}, \hat{Q}_c)$ are given in terms of the bosonic fields $\Theta = \frac{\Theta_\uparrow + \Theta_\downarrow}{\sqrt{2}}$, $\Phi = \frac{\Phi_\uparrow + \Phi_\downarrow}{\sqrt{2}}$ and the zero mode fermionic fields $\hat{\alpha}, \hat{Q}_c$:

$$H_c^{n\neq 0}(\Theta, \Phi; \hat{\alpha}, \hat{Q}_c) = v\hbar\left[\int_{-L/2}^{L/2} dx \left[\frac{K}{2}(\partial_x\Phi(x))^2 + \frac{1}{2K}(\partial_x\Theta(x))^2 - g\cos\left[\sqrt{8\pi}\Theta(x) + \hat{\alpha} + \left(4k_F(V_G) + \frac{2\pi}{L}\hat{Q}_c\right)x\right]\right]\right] + \frac{e^2}{\pi\kappa_0}\int_{-L/2}^{L/2}\int_{-L/2}^{L/2} dx\, dx'\, \partial_x\Theta(x)\left[\frac{e^2}{\sqrt{(x-x')^2 + d^2}} - \frac{e^2}{\sqrt{(x-x')^2 + \xi^2}}\right]\partial_{x'}\Theta(x') \quad (4)$$

where v is the charge velocity $vK = v_F = \frac{\hbar K_F(V_G)}{m*}$ and $K = K(U, n_e)$ is the charge interaction parameter. The last term in equation (4) represents the *forward* part of the long range interaction given in equation (1) with the screening length ξ. The long range interaction is controlled by the coupling constant $\gamma = \frac{e^2}{\hbar c}\cdot\frac{1}{\kappa_0}$, where c is the light velocity and $\kappa_0 = 13.18$ is the dielectric constant for GaAs. The strength of the umklapp interaction g is determined by two parts: the short range Hubbard U repulsive interaction and the large momentum transfer of the Coulomb interaction obtained after the projection. The spin density wave excitations are given by the Hamiltonian $H_s^{n\neq 0}(\Theta_s, \Phi_s; \hat{\alpha}_s, \hat{Q}_s)$ with the spin density wave operators: $\Theta_s = \frac{\Theta_\uparrow - \Theta_\downarrow}{\sqrt{2}}$, $\Phi_s = \frac{\Phi_\uparrow - \Phi_\downarrow}{\sqrt{2}}$

$$H_s^{n\neq 0}(\Theta_s, \Phi_s; \hat{\alpha}_s, \hat{Q}_s) = v_s\hbar\left[\int_{-L/2}^{L/2} dx \left[\frac{K_s}{2}(\partial_x\Phi_s(x))^2 + \frac{1}{2K_s}(\partial_x\Theta_s(x))^2 + g_s\cos\left(\sqrt{8\pi}\Theta_s(x) + \hat{\alpha}_s + \frac{2\pi}{L}\hat{Q}_s x\right)\right]\right] \quad (5)$$

where $v_s = \frac{v_F}{K_s} < v$ is the spin wave velocity, $K_s > 1$ is the spin stiffness and g_s is the spin density wave coupling constant. Next we present the zero mode Hamiltonian $H^{(n=0)}$ using the *normal order* notation: $: H^{(n=0)} :\equiv H^{(n=0)} - \langle F|H^{(n=0)}|F\rangle$ where $|F\rangle$ is the unperturbed Fermi surface at zero temperature given in terms of shifted operators, $N_{R,\sigma} = \hat{N}_{R,\sigma} + \langle F|N_{R,\sigma}|F\rangle$; $N_{L,\sigma} = \hat{N}_{L,\sigma} + \langle F|N_{L,\sigma}|F\rangle$ (see appendix A). The normal order, zero mode Hamiltonian takes the form: $: H^{(n=0)} :=: H_0^{(n=0)} : + : H_{int}^{(n=0)} :$.

$$: H_0^{(n=0)} := \frac{hv_F}{2L}[\hat{N}_{R,\sigma=\uparrow}^2 + \hat{N}_{L,\sigma=\uparrow}^2 + \hat{N}_{R,\sigma=\downarrow}^2 + \hat{N}_{L,\sigma=\downarrow}^2] \quad (6)$$

$$: H_{int}^{(n=0)} := u^{(c)}(L)[(\hat{N}_{R,\sigma=\uparrow} + \hat{N}_{L,\sigma=\uparrow}) + (\hat{N}_{R,\sigma=\downarrow} + \hat{N}_{L,\sigma=\downarrow})]^2 - u^{(s)}(L)[(\hat{N}_{R,\sigma=\uparrow} + \hat{N}_{L,\sigma=\uparrow})^2 - (\hat{N}_{R,\sigma=\downarrow} + \hat{N}_{L,\sigma=\downarrow})^2] + \frac{e^2}{\kappa_0}\frac{1}{2L}F\left(\frac{L}{d}, \frac{\xi}{d}\right) \times [(\hat{N}_{R,\sigma=\uparrow} + \hat{N}_{L,\sigma=\uparrow}) + (\hat{N}_{R,\sigma=\uparrow} + \hat{N}_{L,\sigma=\uparrow})]^2. \quad (7)$$

The zero mode coupling constants obtained from equation (1) are given by the renormalized charge backward interaction $u^{(c)}(L) = \frac{hv_F}{2L}(\frac{1-K^2}{K^2})$ and the backward spin interaction $u^{(s)}(L) = \frac{hv_F}{2L}(\frac{1-K_s^2}{K_s^2})$. At zero temperature and $L \to \infty$, K_s goes to 1 and the backward interaction $u^{(s)}(L)$ vanishes. The function $F(\frac{L}{d}, \frac{\xi}{d}) = \log[\frac{\sqrt{[1+(\frac{d}{L})^2]}+1}{\sqrt{[1+(\frac{d}{L})^2]}-1}] - \log[\frac{\sqrt{[1+(\frac{\xi}{L})^2]}+1}{\sqrt{[1+(\frac{\xi}{L})^2]}-1}]$ is the Fourier transform of the long range screened potential. At finite temperatures, the Fermi energy is shifted by $\delta\mu_0(T)$, which modifies the zero mode Hamiltonian: $\delta H^{(n=0)} = \delta\mu_0(T)[(\hat{N}_{R,\sigma=\uparrow} + \hat{N}_{L,\sigma=\uparrow}) + (\hat{N}_{R,\sigma=\uparrow} + \hat{N}_{L,\sigma=\uparrow})]$.

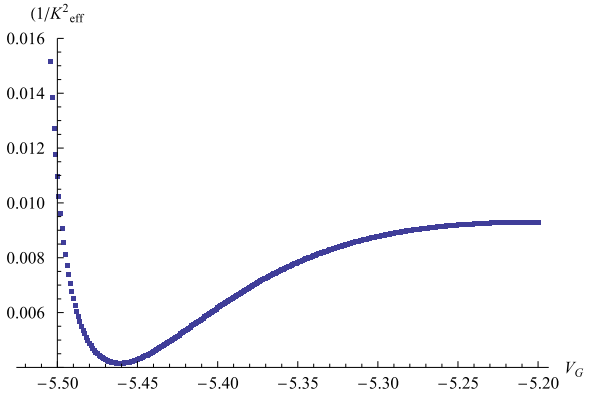

Figure 1. The effective parameter $\frac{1}{K^2_{\rm eff}(l(V_{\rm G}))}$ that is proportional to the inverse compressibility is plotted as a function of the gate voltage $l = l(V_{\rm G})$ for $L = 10^{-6}$ m and the screening ratio $\frac{\xi}{d} = 10$.

5. The renormalization group equations

One of us [30] has developed an RG method which is applicable for the Hamiltonian representation. This method has been used [24] to derive the RG equations for the *unbiased sine-Gordon* model in the presence of long range interactions controlled by the coupling constant $\gamma = \frac{e^2}{\hbar c}\cdot\frac{1}{\kappa_0}$.

$$H_{\rm c}^{n\neq 0}(\Theta,\Phi) = v\hbar\left[\int_{-L/2}^{L/2} {\rm d}x\left[\frac{K}{2}(\partial_x\Phi(x))^2 + \frac{1}{2K}(\partial_x\Theta(x))^2 - g\cos(\sqrt{2n8\pi}\Theta(x))\right]\right] + \frac{e^2}{\pi\kappa_0}\int_{-L/2}^{L/2}\int_{-L/2}^{L/2} {\rm d}x\,{\rm d}x'\,\partial_x\Theta(x) \times\left[\frac{e^2}{\sqrt{(x-x')^2+d^2}}\right]\partial_{x'}\Theta(x'). \quad (8)$$

In the absence of the Coulomb interaction the model is equivalent to the classical two-dimensional sine-Gordon model. According to [33, 34] the model is gapped for $K < \frac{1}{2n}$, $n = 1, 2\ldots$. The long range interaction modifies the results and drives the model to a gapped phase for any value of K. We have extended the RG calculations for the *biased* sine-Gordon model $g\cos[\sqrt{8\pi}\Theta(x) + \hat{\alpha} + (4k_{\rm F}(V_{\rm G}) + \frac{2\pi}{L}\hat{Q}_{\rm c})x]$, given in equation (4). We obtain the *new* RG equations as a function of the *bias* and the *screening* length ξ for the differential momentum shell ${\rm d}l = -\frac{{\rm d}\Lambda}{\Lambda}$.

$$\left(4k_{\rm F}(V_{\rm G}) + \frac{2\pi}{L}\hat{Q}_{\rm c}\right) \to \left(4k_{\rm F}(V_{\rm G}) + \frac{2\pi}{L}\hat{Q}_{\rm c}\right){\rm e}^{l} \quad (9)$$

$$\frac{{\rm d}\hat{g}_{\rm R}(l)}{{\rm d}l} = 2\hat{g}_{\rm R}(l)\left(1 - \frac{K_{\rm R}(l)}{\sqrt{(1+\gamma(\frac{c}{v_{\rm R}(l)})M_{\rm R}(l))}} - \frac{K_{\rm R}^2(l)\hat{g}_{\rm R}^2(l)}{4(1+\gamma(\frac{c}{v_{\rm R}(l)})M_{\rm R}(l))}\right) \quad (10)$$

$$\frac{{\rm d}K_{\rm R}(l)}{{\rm d}l} = -\frac{K_{\rm R}^3(l)\hat{g}_{\rm R}^2(l)}{8(1+\gamma\frac{c}{v_{\rm R}(l)}M_{\rm R}(l))} \quad (11)$$

$$\frac{{\rm d}v_{\rm R}(l)}{{\rm d}l} = \frac{v_{\rm R}(l)K_{\rm R}(l)^2\hat{g}_{\rm R}^2(l)}{4(1+\gamma\frac{c}{v_{\rm R}(l)}M_{\rm R}(l))} \quad (12)$$

where $M_{\rm R}(l)$ is the difference of two Bessel functions $K_0(x)$: $M_{\rm R}(l) = 2(K_0[{\rm e}^{-l}] - K_0[\frac{\xi}{d}\cdot{\rm e}^{-l}])$ The solution of the RG equations depends on the initial values of the interaction parameters $\hat{g}_{\rm R}(l=0)$, $K_{\rm R}(l=0)$ and the ratio $\frac{\xi}{d}$. We will study the case where $4k_{\rm F}(V_{\rm G}) \leqslant \frac{\pi}{d}$. In order to compute the scaling functions, we need to determine the relation between the logarithmic scale l and the voltage $V_{\rm G}$. Based on the experimental observation [3], we have a perfect conductance for a particular gate voltage $V_{\rm G}^{(0)}$ for which the umklapp interaction is negligible. This will happen if $4k_{\rm F}(V_{\rm G}^{(0)})$ corresponds to the momentum $\frac{\pi}{d}$. For this case we find an oscillating behavior for the sine-Gordon term: $g\cos[\sqrt{8\pi}\Theta(x) + \hat{\alpha} + (4k_{\rm F}(V_{\rm G}^{(0)}) + \frac{2\pi}{L}\hat{Q}_{\rm c})x] = g(-1)^n\cos[\sqrt{8\pi}\Theta(x) + \hat{\alpha} + (\frac{2\pi}{L}\hat{Q}_{\rm c})x]$ and can ignore the umklapp contribution. For lower gate voltages $V_{\rm G} < V_{\rm G}^{(0)}$ the situation is different. Following [31] we do not neglect the umklapp interaction for $V_{\rm G} < V_{\rm G}^{(0)}$, instead we compute the effective coupling constant at the length scale $l = l(V_{\rm G})$. This length scale $l = l(V_{\rm G})$ is determined by the equation $4k_{\rm F}(V_{\rm G}){\rm e}^{l(V_{\rm G})} = 4k_{\rm F}(V_{\rm G}^{(0)})$ and is given by $l(V_{\rm G}) = \log[\frac{4k_{\rm F}(V_{\rm G}^{(0)})}{4k_{\rm F}(V_{\rm G})}]$. At this length scale, the renormalized umklapp interaction alternates in sign $g(-1)^n$ and can be neglected if the sine-Gordon coupling constant is small. Using this procedure we substitute the function $l(V_{\rm G})$ into the RG equations and find the renormalized Luttinger parameter as a function of the gate voltage $V_{\rm G}$. Since the wire has a finite length L we stop the scaling when we reach the value $l = {\rm minimum}[l(V_{\rm G}), l_{\rm L}]$, where $l_{\rm L} = \log[\frac{L}{d}]$. In the presence of the Coulomb interactions the Luttinger parameter $K_{\rm R}(l(V_{\rm G}))$ is replaced by the effective parameter $K_{\rm eff}(l(V_{\rm G}))$, computed from the RG equations (9)–(12):

$$K_{\rm eff}(l(V_{\rm G})) = \frac{K_{\rm R}(l(V_{\rm G}))}{\sqrt{1+\gamma\cdot\frac{c}{v_{\rm R}(l(V_{\rm G}))}\cdot\log[(\frac{\xi}{d})^2]}}. \quad (13)$$

The effective interaction parameter $K_{\rm eff}(l(V_{\rm G}))$ decreases monotonically with the decrease in the density and exhibits a maximum for densities where $K_{\rm eff}(l(V_{\rm G})) \approx \frac{1}{2}$. The charge density velocity is enhanced to $v = \frac{v_{\rm F}}{K_{\rm eff}(l(V_{\rm G}))}$. When the screening ratio approaches $\frac{\xi}{d} = 1$, the Coulomb renormalization is absent and $K_{\rm eff}(l(V_{\rm G})) = K_{\rm R}(l(V_{\rm G}))$. In figure 1 we have plotted $\frac{1}{K^2_{\rm eff}(l(V_{\rm G}))}$ as a function of the gate voltage. Following [3], we have used for the gate voltage $V_{\rm G}^{(0)}$ the value $V_{\rm G}^{(0)} = -5.1$ V. We observe that $\frac{1}{K^2_{\rm eff}(l(V_{\rm G}))}$ has a minimum for voltages that corresponds to the region where the 0.7 feature is seen. Since the compressibility κ is proportional to the square of the Luttinger parameter $\kappa \propto K^2_{\rm eff}(l(V_{\rm G}))$, we conclude that a maximum in the compressibility suggests the formation of a gap. (Since the compressibility is proportional to the derivative of the renormalized chemical potential $\mu_{\rm R}(V_{\rm G}, l(V_{\rm G}))$, $\frac{1}{\kappa} = (n_{\rm e}(V_{\rm G}))^2\partial_{n_{\rm e}(V_{\rm G})}[\mu_{\rm R}(V_{\rm G}, l(V_{\rm G}))]$, we also expect a minimum for the derivative.)

6. The effective Hamiltonian $\frac{1}{2} \leqslant K_{\rm eff}(l(V_G)) \leqslant 1$ for $L > \xi$

Using the dependence of the Fermi momentum $k_{\rm F}(V_{\rm G}) < k_{\rm F}(V_{\rm G}^{(0)})$ on the gate voltage $V_{\rm G} < V_{\rm G}^{(0)}$, we find that

the umklapp interaction and the Luttinger parameter are renormalized. Following the analysis from section 5, we find that at the length scale $l(V_G) = \log[\frac{4k_F(V_G^{(0)})}{4k_F(V_G)}]$ the renormalized umklapp interaction is negligible, $g(l(V_G)) \approx 0$, and the renormalized velocity is $\frac{v_F}{K_{eff}(l(V_G))}$. When $L > \xi$, the effective Luttinger parameter is restricted to $\frac{1}{2} \leqslant K_{eff}(l(V_G)) \leqslant 1$. The renormalized bosonic Hamiltonian is given by

$$H^{(n\neq 0)}_{c,l(V_G)}[\Theta_R, \Phi_R] \approx \hbar v_R(l(V_G))\Bigg[\int_{-L/(2e^{l(V_G)})}^{L/(2e^{l(V_G)})} dx \Bigg[\frac{K_R(l(V_G))}{2} \times (\partial_x \Phi_R(x))^2 + \frac{1}{2K_R(l(V_G))}(\partial_x \Theta_R(x))^2\Bigg]\Bigg] + \frac{e^2}{\pi\kappa_0}\int_{-L/(2e^{l(V_G)})}^{L/(2e^{l(V_G)})} dx\, dx'\, \partial_x\Theta_R(x) \times \Bigg[\frac{1}{\sqrt{(x-x')^2 + \left(\frac{d}{e^{l(V_G)}}\right)^2}} - \frac{1}{\sqrt{(x-x')^2 + \left(\frac{\xi}{e^{l(V_G)}}\right)^2}}\Bigg]\partial_{x'}\Theta_R(x') \quad (14)$$

$$H^{n\neq 0}_s(\Theta_s, \Phi_s; \hat{\alpha}_s, \hat{Q}_s, l(V_G)) = \hbar v_{s,R}(l(V_G))\Bigg[\int_{-L/(2e^{l(V_G)})}^{L/(2e^{l(V_G)})} dx \times \Bigg[\frac{K_s(l(V_G))}{2}(\partial_x\Phi_{s,R}(x))^2 + \frac{1}{2K_s(l(V_G))}(\partial_x\Theta_{s,R}(x))^2\Bigg] + g_s(l(V_G))\cos\left(\sqrt{8\pi}\Theta_{s,R}(x) + \hat{\alpha}_s + \frac{2\pi}{L}\hat{Q}_s x e^{l(V_G)}\right)\Bigg]. \quad (15)$$

Since $K_s(l(V_G)) \geqslant 1$, the sine-Gordon scaling shows that $g_s(l(V_G))$ is an irrelevant coupling constant which decreases with the increase of $l(V_G)$. The renormalized zero mode Hamiltonian will depend on the renormalized coupling constants given by the RG equations (9)–(13):

$$:H^{(n=0)}(l(V_G)) :=: H_0^{(n=0)}(l(V_G)) : + H_{int.}^{(n=0)}(l(V_G)). \quad (16)$$

The first term $: H_0^{(n=0)}(l(V_G))$ represents the non-interacting part:

$$: H_0^{(n=0)}(l(V_G)) := \frac{hv_F}{2L} \times [\hat{N}^2_{R,\sigma=\uparrow} + \hat{N}^2_{L,\sigma=\uparrow} + \hat{N}^2_{R,\sigma=\downarrow} + \hat{N}^2_{L,\sigma=\downarrow}]. \quad (17)$$

The second term represents the interactions $: H_{int}^{(n=0)}(l(V_G)) :$, given as a function of the charge operator $Q_c = [(N_{R,\sigma=\uparrow} + N_{L,\sigma=\uparrow}) + (N_{R,\sigma=\downarrow} + N_{L,\sigma=\downarrow})] = \hat{Q}_c + \langle F|Q_c|F\rangle$ and the magnetization operator $Q_s = [(N_{R,\sigma=\uparrow} + N_{L,\sigma=\uparrow}) - (N_{R,\sigma=\downarrow} + N_{L,\sigma=\downarrow})] = \hat{Q}_s + \langle F|Q_s|F\rangle$.

$$: H_{int}^{(n=0)}(l(V_G)) := \eta_c(l(V_G))\hat{Q}_c^2 - \eta_s(l(V_G))\hat{Q}_s^2 \quad (18)$$

where $\eta_c(l(V_G)) \equiv \frac{hv_F}{2L}[(\frac{1-K_R^2(l(V_G))}{K_R^2(l(V_G))}) + \gamma(\frac{c}{v_F})F(\frac{L}{de^{l(V_G)}}, \frac{\xi}{de^{l(V_G)}})]$ are the renormalized backward charge and magnetic interactions $\eta_s(l(V_G)) = \frac{hv_F}{2L}(\frac{1-K^2_{s,R}(l(V_G))}{K^2_{s,R}(l(V_G))})$. Both terms are a function of the screened Coulomb interaction $F(\frac{L}{de^{l(V_G)}}, \frac{\xi}{de^{l(V_G)}})$ given by

$$F\left(\frac{L}{de^{l(V_G)}}, \frac{\xi}{de^{l(V_G)}}\right) = \log\left[\frac{\sqrt{\left[1+\left(\frac{de^{l(V_G)}}{L}\right)^2\right]}+1}{\sqrt{\left[1+\left(\frac{de^{l(V_G)}}{L}\right)^2\right]}-1}\right] - \log\left[\frac{\sqrt{\left[1+\left(\frac{\xi e^{l(V_G)}}{L}\right)^2\right]}+1}{\sqrt{\left[1+\left(\frac{\xi e^{l(V_G)}}{L}\right)^2\right]}-1}\right]. \quad (19)$$

At finite temperatures the effect of the e–e interactions replaces the non-interacting ground state $|F\rangle$ with a shifted Fermi surface given by the renormalized ground state $|G\rangle$. In appendix B we find that the single particle states $\epsilon(n)$ are shifted up in energy by the self-energy $\delta\Sigma(V_G, l(V_G))$. In appendix B we have computed the self-energy $\delta\Sigma(V_G, l(V_G))$ at low temperatures T, which are higher than the spin exchange energy, $K_B T > \eta_s(l(V_G))\langle G|\hat{Q}_s^2|G\rangle = K_B T^*$. $|G\rangle$ is the renormalized Fermi surface, which replaces the non-interacting Fermi surface $|F\rangle$, and T^* is a temperature of the order of 0.05 K. For temperatures $T > T^*$ the self-energy is given by $\delta\Sigma(V_G, l(V_G)) \approx 2\eta_c(l(V_G))\langle G|\hat{Q}_c|G\rangle$ (see appendix B). The effective zero mode Hamiltonian is replaced by

$$: H^{(n=0)}(l)_{eff} :\approx \frac{hv_F}{2L}[\hat{N}^2_{R,\sigma=\uparrow} + \hat{N}^2_{L,\sigma=\uparrow} + \hat{N}^2_{R,\sigma=\downarrow} + \hat{N}^2_{L,\sigma=\downarrow}] + \delta\Sigma(V_G, l(V_G))[\hat{N}_{R,\sigma=\uparrow} + \hat{N}_{R,\sigma=\downarrow} + \hat{N}_{L,\sigma=\uparrow} + \hat{N}_{L,\sigma=\downarrow}]. \quad (20)$$

7. The current for the interacting region $\frac{1}{2} \leqslant K_{eff}(l(V_G)) \leqslant 1, T > T^*$

For finite values of $l(V_G)$ the spin density wave coupling constant $g_s(l(V_G))$ and the spin density wave velocity $v_s(l(V_G)) = \frac{v_F}{K_s(l(V_G))} \ll \frac{v_F}{K_c(l(V_G))} = v(l(V_G))$ are both small. At temperatures $T > T^*$, we replace the interacting zero mode Hamiltonian with the effective zero mode Hamiltonian controlled by the self-energy $\delta\Sigma(V_G, l(V_G))$ given in equation (20). In order to compute the current, we include the reservoir Hamiltonian H_{Res}, controlled by the drain source voltage $V = \frac{\mu^{(0)}_{Left} - \mu^{(0)}_{Right}}{e}$:

$$H_{Res} = \frac{eV}{2}\sum_{\sigma=\uparrow,\downarrow}[(\hat{N}_{L,\sigma} - \hat{N}_{R,\sigma})]. \quad (21)$$

The partition functions in the presence of the reservoir is given by: $Z = T_r[e^{-\beta:H^{(n=0)}(l(V_G))_{eff}:}e^{-\beta:H_{Res}:}] \equiv T_r[e^{-\beta:H_0^{(n=0)}:}e^{-\beta:H^{eff}_{Res}:}]$. The self-energy allows us to replace the reservoir Hamiltonian H_{Res} by an effective reservoir H^{eff}_{Res}:

$$H^{eff}_{Res} = H_{Res} + \sum_{\sigma=\uparrow,\downarrow}[\delta\Sigma(V_G, l(V_G))(\hat{N}_{L,\sigma} + \hat{N}_{R,\sigma})]. \quad (22)$$

The static conductivity is computed using the non-interacting zero mode Hamiltonian $H_0^{(n=0)}$ given in equation (17) and effective reservoir H^{eff}_{Res} given by equation (22). The current is obtained from the derivative of the zero mode coordinate $\hat{\alpha}$

(see section 3), $\hat{I} = \frac{e}{2\pi}\frac{d\hat{\alpha}}{dt}$. Using the Heisenberg equation of motion we obtain the current operator.

$$\hat{I} = \frac{e}{2\pi}\frac{d\hat{\alpha}}{dt} = \frac{e}{i\hbar}[\hat{\alpha}, H_0^{(n=0)}] = \frac{ev_F}{L}\sum_{\sigma=\uparrow,\downarrow}[\hat{N}_{R,\sigma} - \hat{N}_{L,\sigma}]. \tag{23}$$

The thermal expectation function is obtained with the help of the partition function Z.

$$I = T_r[e^{-\beta H_0^{(n=0)}} e^{-\beta H_{Res}^{eff}} \hat{I}][Z]^{-1}. \tag{24}$$

Following appendix A we obtain

$$I = \frac{ev_F}{L}\sum_{\sigma=\uparrow,\downarrow}\sum_{m=-n_F(V_G)}^{m=n_F(V_G)} \times \left(f_{FD}\left[\frac{\epsilon_L(m) + \delta\Sigma(V_G, l(V_G)) + \frac{eV}{2} - \delta\mu_0(T)}{K_B T}\right] - f_{FD}\left[\frac{\epsilon_R(m) + \delta\Sigma(V_G, l(V_G)) - \frac{eV}{2} - \delta\mu_0(T)}{K_B T}\right]\right) \tag{25}$$

where $\epsilon_L(m)$ and $\epsilon_R(m)$ are the single particle energies and $2n_F(V_G)$ is the discrete bandwidth introduced in appendix A. We include a small single particle broadening which will allow us to replace the discrete sum $\epsilon_{R,L}(m)$ by a continuum integration variable ϵ. Performing the integration with respect the energy variable ϵ and expanding with respect the voltage V gives the conductance $G = \frac{I}{V}$:

$$\begin{aligned} G &\approx \frac{2e}{hV}\int_{-\epsilon_F(V_G)}^{\epsilon_F(V_G)} d\epsilon \times \left(f_{FD}\left[\frac{\epsilon + \delta\Sigma(V_G, l(V_G)) + \frac{eV}{2} - \delta\mu_0(T)}{K_B T}\right] - f_{FD}\left[\frac{\epsilon + \delta\Sigma(V_G, l(V_G)) - \frac{eV}{2} - \delta\mu_0(T)}{K_B T}\right]\right) \\ &= \frac{2e^2}{h}\left(f_{FD}\left[\frac{-\epsilon_F(V_G) + \delta\Sigma(V_G, l(V_G)) - \delta\mu_0(T)}{K_B T}\right] - f_{FD}\left[\frac{\epsilon_F(V_G) + \delta\Sigma(V_G, l(V_G)) - \delta\mu_0(T)}{K_B T}\right]\right). \end{aligned} \tag{26}$$

We observe that the self-energy determines the conductance through an effective chemical potential. The bottom of the bandwidth $-\epsilon_F(V_G)$ is replaced by $-\epsilon_F(V_G) + \delta\Sigma(V_G, l(V_G))$. This allows us to introduce the renormalized effective chemical potential $\mu_R(V_G, l(V_G)) = \epsilon_F(V_G) - \delta\Sigma(V_G, l(V_G))$.

8. The strongly interacting region $K_{eff}(l(V_G)) \approx \frac{1}{2}$, $T > T^*$—the effective $U = \infty$ Hubbard model

When $K_{eff}(l(V_G)) \approx \frac{1}{2}$ and $T > T^*$, one obtains an incoherent Luttinger liquid which can be mapped to the Hubbard model $U \to \infty$. (When $U \to \infty$ the interaction Luttinger parameter is given by $K \to \frac{1}{2}$ and the spin excitations, which are of the order $\frac{1}{U}$, can be ignored.) This limit $U \to \infty$ has been considered in the past [29]. In this limit the following constraints must be obeyed: $\psi^+_{\sigma=\uparrow}(x)\psi_{\sigma=\uparrow}(x) + \psi^+_{\sigma=\downarrow}(x)\psi_{\sigma=\downarrow}(x) = 0, 1$. Using the constraints, we have found the following representation [29] for the electron operators: $\psi_\sigma(x) = b_\sigma(x)\Psi(x)$, $\psi^+_\sigma(x) = \Psi^+(x)b^+_\sigma(x)$, where $\Psi(x)$ is the electron charge operator and $b_\sigma(x)$ are the hard core boson for the spin excitations. They obey the constraints: $b^+_{\sigma=\uparrow}(x)b_{\sigma=\uparrow}(x) + b^+_{\sigma=\downarrow}(x)b_{\sigma=\downarrow}(x) = \Psi^+(x)\Psi(x)$. In one dimension, this model has been represented in terms of the bosonic electron operators [29] Θ_e and Φ_e and spinon operators Θ_s and Φ_s. The constraint is imposed on the electron density: $\rho_e(x) \equiv \rho_{\sigma=\uparrow}(x) + \rho_{\sigma=\downarrow}(x) = \frac{1}{\sqrt{\pi}}[\partial_x\Theta_{\sigma=\uparrow}(x) + \partial_x\Theta_{\sigma=\downarrow}(x)] \equiv \frac{1}{\sqrt{\pi}}\partial_x\Theta_e(x)$. The canonical conjugate momentum is given by: $\partial_x\Phi_e(x) \equiv \frac{1}{2}[\partial_x\Phi_{\sigma=\uparrow}(x) + \partial_x\Phi_{\sigma=\downarrow}(x)]$. For non-interacting electrons we have the commutation rule $[\Theta_e(x), \partial_x\Phi_e(y)] = i\hbar\delta(x-y)$. Due to the exclusion of double occupancy, the electronic density is reduced by a factor of two (in comparison with non-interacting electrons) and the commutator is modified to: $[\Theta_e(x), \partial_x\Phi_e(y)]_{Constraint} \approx \frac{i}{2}\hbar\delta(x-y)$.

The Hamiltonian for the $U \to \infty$ case (away from half filling) is given in terms of the fields $\Theta_e(x)$, $\Phi_e(x)$: $H_e = \int dx\, v\hbar[(\partial_x\Phi_e(x))^2 + \frac{1}{4}(\partial_x\Theta_e(x))^2]$.

At finite temperatures, the spinon Hamiltonian $H_s = \int dx \frac{\hbar v}{2}[(\partial_x\Phi_s(x))^2 + (\partial_x\Theta_s(x))^2] \approx 0$ is negligible ($\Theta_s(x) \equiv \frac{1}{\sqrt{2}}[\Theta_{\sigma=\uparrow}(x) - \Theta_{\sigma=\downarrow}(x)]$ and $\Phi_s(x) = \frac{1}{\sqrt{2}}[\Phi_{\sigma=\uparrow}(x) - \Phi_{\sigma=\downarrow}(x)]$). If we inject an electron with a given spin at one lead, we will detect on the other lead a charge with an arbitrary spin. The effect of voltage difference V between the leads is included into the calculation through the reservoir Hamiltonian $\frac{eV}{2\sqrt{\pi}}\int dx\,[\partial_x\Phi_{\sigma=\uparrow}(x) + \partial_x\Phi_{\sigma=\downarrow}(x)] \equiv \frac{eV}{\sqrt{\pi}}\int dx\,\partial_x\Phi_e(x)$. Using the Heisenberg equations of motion with the modified commutator we obtain the electronic current operator [37] $J_e = \frac{ev}{2\sqrt{\pi}}[\partial_x\Phi_{\sigma=\uparrow}(x) + \partial_x\Phi_{\sigma=\downarrow}(x)] \equiv \frac{ev}{\sqrt{\pi}}\partial_x\Phi_e(x)$. The extra factor of $\frac{1}{2}$ which appears in the current operator J_e is due to the commutator $[,]_{Constraint}$ [37]. Therefore, the conductance is reduced to $G \approx \frac{e^2}{h}$.

9. The conductance in the Wigner crystal limit $K_{eff}(l(V_G)) < \frac{1}{2}$

For large screening lengths ξ, the effective Luttinger charge stiffness $K_{eff}(l(V_G))$ decreases below $K_{eff}(l(V_G)) < \frac{1}{2}$ at low temperatures. Under these conditions, the RG analysis reveals that the alternating umklapp coupling constant $g(-1)^n$ generates a gap at $T = 0$. To investigate this region, we introduce two sublattices for the even and odd sites. We replace the bosonic fields by the even and odd combinations: $\Theta_-(y = 2nd) = \frac{\Theta(x=2nd) - \Theta(x=(2n+1)d)}{\sqrt{2}}$ and $\Theta_+(y = 2nd) = \frac{\Theta(x=2nd) + \Theta(x=(2n+1)d)}{\sqrt{2}}$. We integrate out the antisymmetric field $\Theta_-(y = 2nd) = \frac{\Theta(x=2nd) - \Theta(x=(2n+1)d)}{\sqrt{2}}$ and obtain an effective Hamiltonian for the symmetric field $\Theta_+(y = 2nd) = \frac{\Theta(x=2nd) + \Theta(x=(2n+1)d)}{\sqrt{2}}$. The effective Hamiltonian has a set of new coupling constants $|g^{(2)}_{new}| \approx \frac{g^2}{2!}\langle(\sin[\sqrt{4\pi}\Theta_-(y)])^2\rangle$.

$$H_c^{n\neq 0}(\Theta_+, \Phi_+) \approx \hbar v(l(V_G)) \times \left[\int_{-L/2}^{L/2} dy \left[\frac{K_{eff}(l(V_G))}{2}(\partial_y\Phi_+(y))^2\right.\right.$$

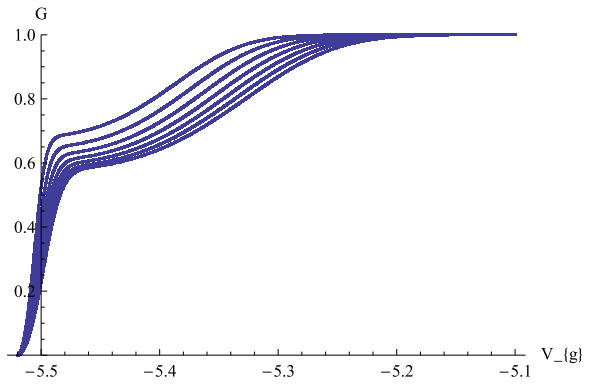

Figure 2. The conductance G in units of $\frac{2e^2}{h}$ as a function of the bias gate voltage $l = l(V_G)$ for the temperatures $T = 1$ K (upper line), $T = 1.25$, 1.5, 1.75, 2.0 , 2.25 , 2.5 and 3 K (the lowest line) for the umklapp parameter $g(l = 0) = 0.05$, $K(l = 0) \approx 0.98$, $L = 10^{-6}$ m and the screening ratio $\frac{\xi}{d} = 10$.

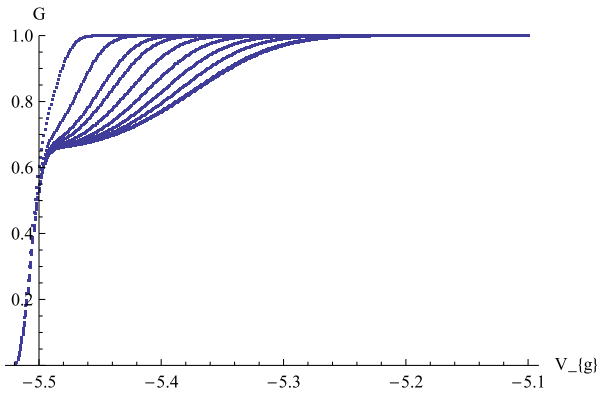

Figure 3. The conductance G in units of $\frac{2e^2}{h}$ for four screening ratios $\frac{\xi}{d} = 1$ (upper line), $\frac{\xi}{d} = 1.1$, 1.3, 1.5, 2, 3, 5, 10, 50 and 100 at temperature $T = 1$ K, length $L = 10^{-6}$ m, for the interaction parameters $\hat{g}_R(l = 0) = 0.05$, $K(l = 0) \approx 0.98$.

$$+\frac{1}{2K_{\rm eff}(l(V_G))}(\partial_y\Theta_+(y))^2 + g^{(2)}_{\rm new,R}(l(V_G))\cos(\sqrt{16\pi}\Theta_+(y))\Big]\Big] \quad (27)$$

where the new coupling constant $g^{(2)}_{\rm new,R}(l(V_G))$ obeys the RG equation.

$$\frac{{\rm d}\hat{g}^{(2)}_{\rm new,R}(l)}{{\rm d}l} = 2\hat{g}^{(2)}_{\rm new,R}(l)[1 - 2K_{\rm eff}(l)]. \quad (28)$$

This equation shows that $\hat{g}^{(2)}_{\rm new,R}(l)$ is a relevant coupling constant for $K_{\rm eff}(l(V_G)) < \frac{1}{2}$. As a result, a charge gap $\Delta \approx \Lambda(\hat{g}^{(2)}_{\rm new})^{\frac{1}{2(2K_{\rm eff}(l(V_G))-1)}}$ will open. When $K_{\rm eff}(l(V_G)) < \frac{1}{2}$, we obtain from equation (28) that at $T = 0$ the expectation value of the phase $\sqrt{16\pi}\langle\Theta_+(x)\rangle = \pi$ will give rise to a Wigner crystal order $\rho(x) \approx$ constant $+ \cos[4k_F x + \frac{\pi}{\sqrt{2}}]{\rm e}^{-\frac{\pi}{2}\langle(\Theta(x)-\langle\Theta(x)\rangle)^2\rangle}$. (Expanding the cosine term in equation (27) around the ground state $\langle\Theta_+(x)\rangle \neq 0$ shows that the charge density wave has a gap Δ. This gap suppresses the fluctuations ${\rm e}^{-\frac{\pi}{2}\langle(\Theta(x)-\langle\Theta(x)\rangle)^2\rangle} \neq 0$ and stabilizes the Wigner Crystal order at $T = 0$.) In order to evaluate the effect of the charge gap Δ on the electronic spectrum, we map [35, 36] the bosonic charge Hamiltonian to a spinless fermion for $K_{\rm eff}(l(V_G)) \approx \frac{1}{2}$. We introduce a two component spinless fermion: $\chi^+(x) = [\chi_1(x), \chi_2(x)]^+ \equiv \sqrt{\frac{\Lambda}{2\pi}}[{\rm e}^{{\rm i}\sqrt{4\pi}\Theta_+(x)}, {\rm e}^{-{\rm i}\sqrt{4\pi}\Theta_+(x)}]^+$. As a result we find for $K_{\rm eff}(l(V_G)) \approx \frac{1}{2}$ that the Hamiltonian in equation (27) is mapped to a spinless fermion model:

$$H_{\rm c,F} = \int {\rm d}x\left[\hbar v(l(V_G))\chi^+(x)(-{\rm i}\partial_x\sigma_3)\chi(x) + \frac{\hat{g}^{(2)}_{\rm new,R}(l(V_G))}{2}(\chi^+(x)\sigma_1\chi(x))^2\right]$$
$$\approx \int {\rm d}x\,[\hbar v(l(V_G))\chi^+(x)(-{\rm i}\partial_x\sigma_3)\chi(x) + \hat{g}^{(2)}_{\rm new,R}(l(V_G))\langle\chi^+(x)\sigma_1\chi(x)\rangle\chi^+(x)\sigma_1\chi(x)] \quad (29)$$

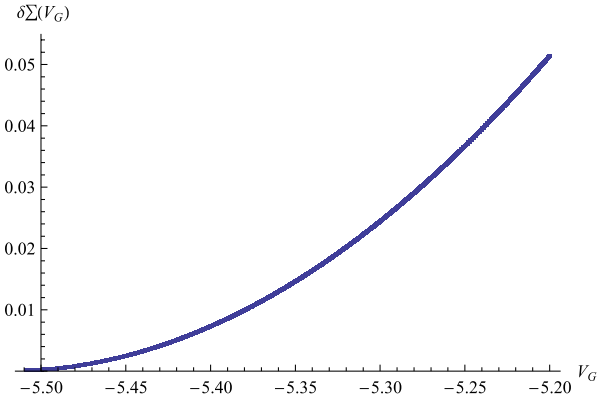

Figure 4. The shift in the chemical potential $\delta\Sigma(V_G, l(V_G))$ for screening ratio $\frac{\xi}{d} = 10$ at temperature $T = 1$ K, length $L = 10^{-6}$ m, for the interaction parameters $\hat{g}_R(l = 0) = 0.05$, $K(l = 0) \approx 0.98$.

where σ_3 and σ_1 are the Pauli matrices. As a result, we have a gap $2\hat{\Delta}$ between the lower band and the upper band given by the self-consistent solution: $\Delta \approx \hat{\Delta} = \hat{g}^{(2)}_{\rm new,R}(l(V_G))\langle\chi^+(x)\sigma_1\chi(x)\rangle$. The energy difference Δ between the Fermi energy and the top of the lower electronic band will affect the conductance through the Fermi–Dirac function. For this case, the self-energy is replaced by the gap Δ and the conductance is approximated by $G \approx \frac{2e^2}{h}[1 - f_{\rm FD}(\frac{\Delta}{K_B T})]$; for $K_B T \geqslant \Delta$ the conductance is given by $G \approx \frac{e^2}{h}$.

10. Numerical results

We have used the experimental relation between the Fermi momentum and the gate voltage V_G given by $K_F(V_G) = \frac{\pi}{2}n_e(V_G) = \frac{C_a}{e}(V_G - V^{\rm th})$, $V^{\rm th} \approx -5.52$ V, $\frac{C_a}{e} = 1.2 \times 10^8$ (V m)$^{-1}$ [3] to compute the conductance in figures 2 and 3. In figure 2 we have considered a typical screening ratio $\frac{\xi}{d} = 10$ and plotted the conductance for a varying range of temperatures 1–3 K. Figure 3 shows the conductance at a fixed temperature $T = 1$ K for different screening lengths. We observe that for $\frac{\xi}{d} = 1$, the Coulomb interaction is

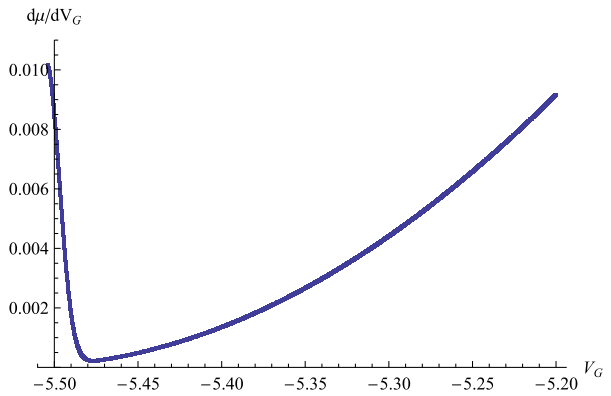

Figure 5. The derivative of the chemical potential $\frac{d\mu_R(V_G,l(V_G))}{dV_G}$ for screening ratio $\frac{\xi}{d} = 10$ at temperature $T = 1$ K, length $L = 10^{-6}$ m, for the interaction parameters $\hat{g}_R(l = 0) = 0.05$, $K(l = 0) \approx 0.98$.

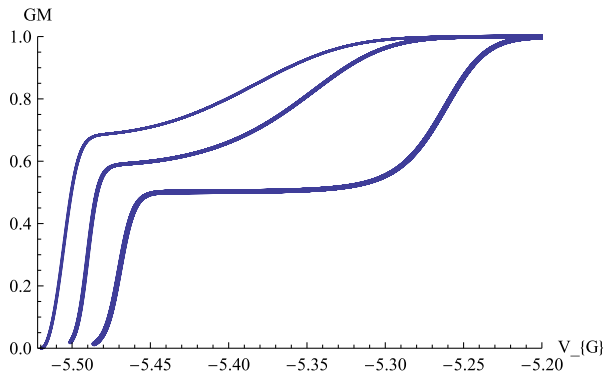

Figure 6. The effect of the magnetic field on the conductance in units $2e^2/h$. The first graph represents the conductance for zero magnetic field, the second graph represents the conductance for a magnetic field $B = 3$ T and the third graph represents the conductance for the magnetic field $B = 10$ T. The other parameters were: screening ratio $\frac{\xi}{d} = 10$, temperature $T = 1$ K, length $L = 10^{-6}$ m, $d = 10^{-8}$ m, $\hat{g}_R(l = 0) = 0.05$ and $K(l = 0) \approx 0.98$.

completely screened and the 0.7 feature is absent. In figure 4, we plot the dependence of the self-energy $\delta\Sigma(V_G, l(V_G))$ on the gate voltage V_G. We observe that at low densities the free energy has an extremum at a finite density. The renormalized chemical potential $\mu_R(V_G, l(V_G)) = \epsilon_F(V_G) - \delta\Sigma(V_G, l(V_G))$ vanishes at the voltage $V_G^* > V^{th}$. For $V^{th} < V_G < V_G^*$, the renormalized chemical potential is negative, indicating the formation of a charge density wave gap at $T = 0$ for $K_{eff}(l(V_G)) < \frac{1}{2}$. The derivative of the conductance and chemical potential are related to the inverse compressibility: $\frac{dG(V_G)}{dV_G} \propto \frac{d\mu_R(V_G,l(V_G))}{dV_G} \propto \frac{1}{n_e^2(V_G)\kappa(V_G)}$. The 0.7 anomaly is translated into a minimum around $V_G = -5.49$ V for the conductance derivative $\frac{dG(V_G)}{dV_G}$ and the compressibility $\kappa(V_G)$, which is proportional to the inverse square of the effective interaction parameter $K_{eff}(l(V_G))$ shown in figure 1. Therefore, we have the confirmation for the formation of a charge density wave gap for $K_{eff}(l(V_G))$, $\frac{1}{2}$ at zero temperature. In figure 5, we plot the function $\frac{d\mu_R(V_G,l(V_G))}{dV_G}$. This function has a minimum at the voltage $V_G = -5.49$ V, which corresponds to the $0.7\frac{2e^2}{h}$ structure observed for the conductance graph.

11. The effect of the Zeeman magnetic field

The *Zeeman magnetic* field [2] introduce a bias term $2(k_F^{\uparrow}(V_G)) - (k_F^{\downarrow}(V_G))x$ into the last term in equation (5). Expressing the bias in terms of the magnetic field $B_{||}$ we find, $2(k_F^{\uparrow}(V_G)) - (k_F^{\downarrow}(V_G)) = 2k_F(V_G)(\sqrt{1+\frac{\Delta_z}{2\mu_F}} - \sqrt{1-\frac{\Delta_z}{2\mu_F}}) \approx 4k_F(V_G)(\frac{\Delta_z}{2\mu_F})$, where $\mu_F = \frac{\hbar^2 k_F^2(V_G)}{2m^*}$ is the Fermi energy and $\Delta_z = g_{||}\mu_B B_{||}$ is the Zeeman energy. As a result the spin part sine-Gordon term vanishes, since $K_s(l) > 1$. As a result the spin wave velocity $v_s = \frac{v_F}{K_s}$ is further reduced. For large magnetic fields $\frac{\Delta_z}{2\mu_F} > 1$, the wire will be polarized and we will have only one propagating channel with the conductance $G \approx 0.5 \times (2e^2/h)$.

The effect on the charge density wave Hamiltonian will be to replace $4k_F(V_G)$ in equation (4) by: $2[k_F^{\uparrow}(V_G) + k_F^{\downarrow}(V_G)] \equiv 4k_F(V_G)[\sqrt{1+\frac{\Delta_z}{2\mu_F}} + \sqrt{1-\frac{\Delta_z}{2\mu_F}}]\frac{1}{2}$. For $\frac{\Delta_z}{2\mu_F} < 1$ we show that the perfect conductance in the absence of the Zeeman magnetic field computed at the gate voltage V_G^0 is shifted to a larger gate voltage $V_G^{0-Zeeman}$ in the presence of the Zeeman field: $2[k_F^{\uparrow}(V_G^{0-Zeeman}) + k_F^{\downarrow}(V_G^{0-Zeeman})] \approx 4k_F(V_G^{0-Zeeman})[1 - \frac{1}{8}(\frac{\Delta_z}{2\mu_F})^2] = 4k_F(V_G^0) = \frac{\pi}{d}$. This formula shows the shift in the perfect conductance from $4k_F(V_G^0) = \frac{\pi}{d}$ to a larger gate voltage $V_G^{(0-Zeeman)} > V_G^0$, given by $k_F(V_G^{(0-Zeeman)}) \approx \frac{k_F(V_G^0)}{1-\frac{1}{8}(\frac{\Delta_z}{2\mu_F})^2}$. This result is in agreement with the experimental observations [2].

The conductance at finite temperatures $T > T^*$ will be given by replacing the self-energy in equation (26) with a new self-energy computed in the presence of the magnetic field, $\epsilon_{F,\sigma=\uparrow}(V_G) = \epsilon_F(V_G) + \frac{\Delta_z}{2}$ and $\epsilon_{F,\sigma=\downarrow}(V_G) = \epsilon_F(V_G) - \frac{\Delta_z}{2}$. The results for the conductance are shown in figure 6. We show three graphs: the first graph (thin line) represents the conductance in the absence of the magnetic field and the other two graphs represent the conductance for the magnetic fields $B = 3$ and 10 T. We observe a shift of the conductance to higher voltages with an increase of the magnetic field.

12. Conclusion

We have presented a model which explains the conductance anomaly at finite temperatures as a function of the gate voltage. Due to the Coulomb long range interactions a weakly interacting electronic system can flow to the strong coupling limit $K_{eff}(l(V_G)) < \frac{1}{2}$. When the screening length is not too large, the Luttinger stiffness is restricted to $\frac{1}{2} \leqslant K_{eff}(l(V_G)) < 1$. As a result, the conductance of an infinite wire is perfect at zero temperature. At temperatures larger than the magnetic exchange energy $T > T^*$, we have an incoherent Luttinger model. For $K_{eff}(l(V_G)) \approx \frac{1}{2}$ the interacting wire is equivalent to the Hubbard $U \to \infty$ model with the anomalous conductance $G \approx \frac{e^2}{h}$.

For large screening lengths the interacting charge stiffness decreases to $K_{eff}(l(V_G)) < \frac{1}{2}$. As a result we find that at zero temperature we have a Wigner crystal with a charge gap Δ. At finite temperatures the formation of charge density

wave gap gives rise to the anomalous conductance $G \approx \frac{2e^2}{h}[1 - f_{\rm FD}(\frac{\Delta}{K_{\rm B}T})]$. Following [2] we have investigated the effect of the magnetic field. We have shown that the magnetic field shifts the region of the perfect conductance to higher voltages.

Some of the concepts used in our work are common to other theories [38, 39]. The long range interactions have been introduced by [12, 14]; in the present paper we show that, by varying the gate voltage and screening length we obtain either a strongly interacting metal or a Wigner crystal. Other theories use a weak scattering potential [8] or charge localization [9, 40] and are consistent with our picture. In our view the origin of the scattering potential (microscopic or phenomenological) is not crucial! The crucial effect is that any weak scattering is strongly enhanced by the long range interactions! Our findings show that, due to the long range interaction, any negligible scattering potential is enhanced and eventually can drive the system to an insulating regime. It is the interplay between the screening length, gate voltage and temperature which gives rise to the conductance anomaly. One of the popular theories is based on the Kondo model [4, 9]. The *Kondo* picture dictates that the anomaly should be observed above the Kondo temperature. When the temperature is lowered below the Kondo temperature, the conductance is restored to the universal value. This picture is consistent with our theory in the following way: if the strong coupling regime $K_{\rm eff}(l(V_{\rm G})) \approx \frac{1}{2}$ is reached in the metallic phase, we can use the Hubbard $U \to \infty$ limit, which is the basis for deriving the Kondo model. The Kondo physics emerges for finite exchange coupling $J \propto \frac{1}{U}$. In our case, the anomalous conductance is observed at finite temperatures $T > T^*$, which is comparable to $\frac{1}{U}$ where the Kondo picture emerges.

Acknowledgments

D Shmeltzer wants to thank Dr Jing Qiao Zhang for his invaluable help and guidance with the computational part and graphical presentation of this work. The authors acknowledge the financial support from the CUNY Collaborative Grant award for the year 2007–2008.

Appendix A

The non-interacting Fermi surface at $T = 0$ is given by the state $|F\rangle$, which is constructed from the vacuum $|0\rangle$: $|F\rangle \equiv \prod_{\sigma=\uparrow,\downarrow}[\prod_{-n_{\rm F}(V_{\rm G})}^{n_{\rm F}(V_{\rm G})} R^+(m,\sigma) \prod_{n_{\rm F}(V_{\rm G})}^{-n_{\rm F}(V_{\rm G})} L^+(m,\sigma)]|0\rangle$. We introduce the notation $\hat{N}_{{\rm R},\sigma}\hat{N}_{{\rm L},\sigma}$ for the normal order at zero temperature:

$$\begin{aligned}\hat{N}_{{\rm R},\sigma} &= \sum_{-n_{\rm F}(V_{\rm G})}^{n_{\rm F}(V_{\rm G})} R^+(m,\sigma)R(n,\sigma) \\ &\quad - \sum_{-n_{\rm F}(V_{\rm G})}^{n_{\rm F}(V_{\rm G})} \langle F|R^+(m,\sigma)R(m,\sigma)|F\rangle \\ &\equiv N_{{\rm R},\sigma} - \langle F|N_{{\rm R},\sigma}|F\rangle \end{aligned} \tag{30}$$

$$\begin{aligned}\hat{N}_{{\rm L},\sigma} &= \sum_{n_{\rm F}(V_{\rm G})}^{-n_{\rm F}(V_{\rm G})} L^+(m,\sigma)L(m,\sigma) \\ &\quad - \sum_{n_{\rm F}(V_{\rm G})}^{-n_{\rm F}(V_{\rm G})} \langle F|L^+(m,\sigma)L(m,\sigma)|F\rangle \\ &= N_{{\rm L},\sigma} - \langle F|N_{{\rm L},\sigma}|F\rangle. \end{aligned} \tag{31}$$

The presence of a reservoir with two chemical potentials $\mu_{\rm R}$ and $\mu_{\rm L}$ is described by the reservoir Hamiltonian:

$$\begin{aligned}H_{\rm Res} &= \mu_{\rm R} \sum_{-n_{\rm F}(V_{\rm G})}^{n_{\rm F}(V_{\rm G})} R^+(m,\sigma)R(m,\sigma) \\ &\quad + \mu_{\rm L} \sum_{-n_{\rm F}(V_{\rm G})}^{n_{\rm F}(V_{\rm G})} L^+(m,\sigma)L(m,\sigma). \end{aligned} \tag{32}$$

At finite temperatures, the Fermi surface is shifted by $\delta\mu_0(T)$ and is given (for the one-dimensional case) by: $\delta\mu_0(T) = \epsilon_{\rm F}(V_{\rm G})\frac{\pi^2}{12}(\frac{K_{\rm B}T}{\epsilon_{\rm F}(V_{\rm G})})^2$. The temperature and the reservoir modifies the number of fermions in the thermal ground state to $\langle N_{{\rm R},\sigma}(V_{\rm G},\mu_{\rm R},T)\rangle$ and $\langle N_{{\rm L},\sigma}(V_{\rm G},\mu_{\rm L},T)\rangle$ given by:

$$\langle N_{{\rm R},\sigma}(V_{\rm G},\mu_{\rm R},T)\rangle = \sum_{n_{\rm F}(V_{\rm G})}^{-n_{\rm F}(V_{\rm G})} f_{\rm FD}\left[\frac{\epsilon_{\rm R}(m) - \mu_{\rm R} - \delta\mu_0(T)}{K_{\rm B}T}\right] \tag{33}$$

$$\langle N_{{\rm L},\sigma}(V_{\rm G},\mu_{\rm L},T)\rangle = \sum_{n_{\rm F}(V_{\rm G})}^{-n_{\rm F}(V_{\rm G})} f_{\rm FD}\left[\frac{\epsilon_{\rm L}(m) - \mu_{\rm L} - \delta\mu_0(T)}{K_{\rm B}T}\right]. \tag{34}$$

The expectation value of the normal order operators will be given by:

$$\begin{aligned}\langle\hat{N}_{{\rm L},\sigma}(V_{\rm G},\mu_{\rm L},T)\rangle &= \langle N_{{\rm L},\sigma}(V_{\rm G},\mu_{\rm L},T)\rangle \\ &\quad - \langle N_{{\rm L},\sigma}(\delta\mu_0(T),T)\rangle; \\ \langle\hat{N}_{{\rm R},\sigma}(V_{\rm G},\mu_{\rm R},T)\rangle &= \langle N_{{\rm R},\sigma}(V_{\rm G},\mu_{\rm R},T)\rangle \\ &\quad - \langle N_{{\rm R},\sigma}(\delta\mu_0(T),T)\rangle. \end{aligned}$$

The effect of the self-energy $\delta\Sigma(V_{\rm G},l(V_{\rm G}),T)$ will be taken in consideration by substituting in the previous equations: $\mu_{\rm R} \to \mu_{\rm R} - \delta\Sigma(V_{\rm G},l(V_{\rm G}),T)$ and $\mu_{\rm L} \to \mu_{\rm L} - \delta\Sigma(V_{\rm G},l(V_{\rm G}),T)$.

Appendix B

The purpose of this appendix is to compute the self-energy $\delta\Sigma(V_{\rm G},l(V_{\rm G}),T)$ for the following model:

$$:H_{\rm int}^{(n=0)}(l) := \eta_{\rm c}(l(V_{\rm G}))\hat{Q}_{\rm c}^2 - \eta_{\rm s}(l(V_{\rm G}))\hat{Q}_{\rm s}^2 \tag{35}$$

where $Q_{\rm c} = \hat{Q}_{\rm c} + \langle F|Q_{\rm c}|F\rangle$ is the charge operator and $Q_{\rm s} = \hat{Q}_{\rm s} + \langle F|Q_{\rm s}|F\rangle$ is the magnetization operator. We observe that the zero mode component of the Hamiltonian commutes: $[H_0^{(n=0)}(l), H_{\rm int}^{(n=0)}(l)] = 0$. Therefore, at finite temperatures, the partition function $Z^{(n=0)} = T_r[{\rm e}^{-\beta H^{(n=0)}(l)}]$ can be computed exactly. Our goal is to compute the charge current $\hat{I} = e\frac{{\rm d}\hat{\alpha}}{{\rm d}t}$, which is given by the commutator $[\hat{\alpha}, H^{(n=0)}(l)]$. We will limited ourselves to finite temperatures such that the exchange energy is smaller than the thermal energy and, therefore, can be ignored (for long wires the spin

stiffness approaches $K_s \approx 1$ and the last term in equation (19) $\eta_s(l(V_G))$ vanishes). We will compute the self-energy at finite temperature $\delta\Sigma(V_G, l(V_G))$. For the non-interacting ground state $|F\rangle$ with the electronic density $n_e(V_G)$ we have at a temperature T the equation: $n_e(V_G) = \frac{\langle F|Q_c|F\rangle}{L} = \frac{4}{L}\sum_{m=-n_F(V_G)}^{m=n_F(V_G)} f_{FD}[\frac{\epsilon(m)-\delta\mu_0(T)}{K_B T}]$. The effect of the interactions will replace the ground state $|F\rangle$ by the renormalized ground state $|G\rangle$. The ground state represents a shifted Fermi Surface given by the self-energy $\delta\Sigma(V_G, l(V_G))$ determined by the self-consistent equation:

$$\delta\Sigma(V_G, l(V_G)) = 2\eta_c(l(V_G))\langle G|\hat{Q}_c|G\rangle \equiv 2\eta_c(l(V_G))4 \sum_{m=-n_F(V_G)}^{m=n_F(V_G)} f_{FD} \times \left[\frac{\epsilon(m) + \delta\Sigma(V_G, l(V_G)) - \delta\mu_0(T)}{K_B T}\right]. \quad (36)$$

The solution for $\delta\Sigma(V_G, l(V_G))$ is obtained once we replace the sum by an energy integration (the density of states cancel the velocity):

$$\delta\Sigma(V_G, l(V_G)) \equiv h v_F \left[\left(\frac{1 - K_R^2(l(V_G))}{K_R^2 l(V_G)}\right) + \gamma\left(\frac{c}{v_F}\right) F\left(\frac{L}{d e^{l(V_G)}}, \frac{\xi}{d e^{l(V_G)}}\right)\right] \cdot \frac{n_e(V_G)}{\hat{\epsilon}(V_G, l, T, L)} \quad (37)$$

where the explicit form $\hat{\epsilon}(V_G, l, T, L)$ represents the effective dielectric function given by

$$\hat{\epsilon}(V_G, l, T, L) = 1 + 4\left[\frac{1 - K_R^2(l(V_G))}{K_R^2(l(V_G))} + \gamma\left(\frac{c}{v_F}\right) F\left(\frac{L}{d e^{l(VG)}}, \frac{\xi}{d e^{l(VG)}}\right) \cdot r(T)\right] \quad (38)$$

where $r(T)$ represents the thermal correction, which is 1 when we use the approximation: $\int_{\epsilon_F(V_G)-\delta\Sigma(V_G,l(V_G))}^{\epsilon_F(V_G)+\delta\Sigma(V_G,l(V_G))} d\epsilon\, f_{FD}[\frac{\epsilon-\delta\mu_0(T)}{K_B T}] \approx 0$. When the self-energy is small with respect to the Fermi energy $\frac{\delta\Sigma(V_G,l(V_G))}{\epsilon_F(V_G)} \ll 1$, we expand the Fermi–Dirac function with respect to $\delta\Sigma(V_G, l(V_G))$ and find: $r(T) = f_{FD}[\frac{-\epsilon_F(V_G)-\delta\mu_0(T)}{K_B T}] - f_{FD}[\frac{\epsilon_F(V_G)-\delta\mu_0(T)}{K_B T}]$.

References

[1] Thomas K J, Nichols J T, Appleyard N J, Simmons M Y, Pepper M, Mace D R and Ritchie D A 1996 *Phys. Rev. Lett.* **77** 135

[2] Thomas K J, Nichols J T, Appleyard N J, Simmons M Y, Pepper M, Mace D R, Tribe W R and Ritchie D A 1998 *Phys. Rev.* B **58** 4826

[3] de Picciotto R *et al* 2005 *Phys. Rev.* B **72** 033319

[4] Cronennwett S M *et al* 2002 *Phys. Rev. Lett.* **88** 226805

[5] Yoon Y, Mourokh L, Morimoto T, Aoki N, Ochiai Y, Reno J L and Bird J P 2007 *Phys. Rev. Lett.* **99** 136805

[6] Komijani Y *et al* 2009 arXiv:0908.2360 [cond-mat]

[7] Bruus H, Cheianov V V and Flensberg K 2001 *Physica* E **10** 97

[8] Reilly D J 2005 *Phys. Rev.* B **72** 033309

[9] Hirose K *et al* 2004 *Phys. Rev. Lett.* **90** 026804

[10] Schmeltzer D *et al* 1998 *Phil. Mag.* B **77** 1189

[11] Sushkov O P 2003 *Phys. Rev.* B **67** 195318

[12] Matveev K A 2004 *Phys. Rev.* B **70** 245319

[13] Aryanpour K and Han J E 2009 *Phys. Rev. Lett.* **102** 056805

[14] Meyer J S and Matveev K A 2009 *J. Phys.: Condens. Matter* **21** 023203 (arXiv:0808.2076)

[15] Fiete G A 2007 *Rev. Mod. Phys.* **79** 801

[16] Cheianov V V and Zvonarev M B 2004 *Phys. Rev. Lett.* **92** 176401

[17] Syljuasen O F 2007 *Phys. Rev. Lett.* **98** 166401

[18] Rejec T and Meir Y 2006 *Nature* **442** 900

[19] Haldane F D M 1981 *J. Phys. C: Solid State Phys.* **14** 2585
Haldane F D M 1981 *Phys. Rev. Lett.* **47** 1840

[20] Kane C L and Fisher M P A 1992 *Phys. Rev.* B **46** 15233

[21] Safi I and Shulz H J 1995 *Phys. Rev.* B **52** R17040

[22] Schmeltzer D 2001 *Phys. Rev.* B **63** 1253321
Schmeltzer D 2000 *Phys. Rev. Lett.* **85** 4132

[23] Maslov D L and Stone M 1995 *Phys. Rev.* B **52** R5539

[24] Malard M, Schmeltzer D and Kuklov A 2009 *Physica* B **404** 3155–8

[25] Shultz H J 1993 *Phys. Rev. Lett.* **71** 1864

[26] Schmeltzer D *et al* 2005 *Phys. Rev.* B **71** 045429
Schmeltzer D *et al* 2005 *Phys. Rev. Lett.* **95** 06880

[27] Di Francesco P, Mathieu P and Senechal D 1996 *Conformal Field Theory* (Berlin: Springer) p 390

[28] Kawakami N and Yang S K 1991 *J. Phys.: Condens. Matter* **3** 5983

[29] Schmeltzer D 1991 *Phys. Rev.* B **43** 8650
Schmeltzer D and Bishop A R 1992 *Phys. Rev.* B **45** 3168

[30] Schmeltzer D 2002 arXiv:cond-mat/0211449,v1

[31] Sun P and Schmeltzer D 2000 *Phys. Rev.* B **61** 349

[32] Shankar R 1990 *Int. J. Mod. Phys.* B **4** 2371

[33] Kosterlitz J M and Thouless D 1972 *J. Phys. C: Solid State Phys.* **5** L124

[34] Berezinskii V L 1972 *Sov. Phys.—JETP* **34** 610

[35] Luther A and Emery V J 1974 *Phys. Rev. Lett.* **33** 589

[36] Mori M, Gata M O and Fukuyama H 1996 *J. Phys. Soc. Japan* **65** 3604
Mori M, Gata M O and Fukuyama H 1997 arXiv:cond-mat/970802

[37] Schmeltzer D 2010 arXiv:1001.2338 [cond-mat]

[38] Pepper M and Bird J 2008 *J. Phys.: Condens. Matter* **20** 160301

[39] Rech J and Matveev K A 2008 *J. Phys.: Condens. Matter* **20** 164211

[40] Meir Y 2008 *J. Phys.: Condens. Matter* **20** 164208